

Power Quality Constrained Optimal Management of Unbalanced Smart Microgrids During Scheduled Multiple Transitions Between Grid-Connected and Islanded Modes

Karim Hassan Youssef

Index Terms—Power quality (PQ), demand response (DR), distribution optimal power flow (DOPF).

NOMENCLATURE

Δf	Frequency deviation from nominal frequency in Hz.
λ_g	Required ratio between power set point of generators g , and $g + 1$.
ϕ_h^n	Phase angle of harmonic current of order h at bus n with respect to fundamental current.
ξ_s	Energy storage efficiency.
B	Set of all network buses.
C	Set of all consumers with controllable loads.
CE	Set of all controllable loads with energy storage.
d_g	Damping coefficient of generator g including local frequency-dependent load in kW/Hz.
E_i	Energy consumption of controllable load i in kWh.
f_{total}	Total objective function.
f_c^t, f_r^t	Price of energy purchased from/sold to grid in \$/kWh.

f_{cr}^t, f_d^t	Cost of reducing power of the critical and ordinary load in \$/kW.
f_g^t	Linear cost coefficient of generator g in \$/kW.
f_i	Cost of reduction of controllable load i in \$/ kWh.
G	Set of all conventional generators.
GM	Set of time slots of grid-connected mode.
h_g^t	Quadratic cost coefficient of generator g in \$/kW ² .
IM	Set of hours of islanded mode.
I_{grid}^t	Three-phase grid currents at fundamental frequency.
I_h^t	Injected bus currents vector of harmonic order h .
I_L^t	Fundamental injected load currents vector.
K_h	Harmonic characteristic matrix at order h .
k_t	Time of the last islanding start before time slot t .
N	Set of all three-phase lines.
N_b	Set of all three-phase lines connected to bus b .
n_L	Number of load (non-grid) buses.
P_n^t	Fundamental active power injected at node n .
P_{cr}^t, P_d^t	Critical and ordinary load power in kW.
P_g^t	Generated power of generator g in kW.
P_{grid}^t	Active power imported from grid in kW.
P_i^t	Consumed power of controllable consumer i .
P_s^t, P_w^t	Maximum available PV and wind power in kW.
Q_n^t	Fundamental reactive power injected at node n .
q_d^t	Reactive power of ordinary load in kVar.
q_g^t	Reactive power of generator g in kVar.
q_{grid}^t	Reactive power imported from grid in kVar.
r_g	Droop constant of generator g in kW/Hz.
SE_i^t	Energy Storage of consumer i in kWh.
S_{gmax}	Rating of conventional generator g in KVA.
S_{Tmax}	Rating of the transformer at PCC in KVA.
THD_n^t	Voltage THD at bus n .
TM	Set of all scheduling time slots.

Manuscript received April 19, 2015; revised March 6, 2016, May 3, 2016, and May 18, 2016; accepted June 5, 2016. Date of publication June 7, 2016; date of current version December 21, 2016. Paper no. TSG-00444-2015.

The author is with the Electrical Engineering Department, Faculty of Engineering, Alexandria University, Alexandria 21544, Egypt (e-mail: khmyoussef@yahoo.com).

Color versions of one or more of the figures in this paper are available online at <http://ieeexplore.ieee.org>.

Digital Object Identifier 10.1109/TSG.2016.2577643

u_h^n	Ratio of harmonic current magnitude of order h at bus n to fundamental current magnitude.
V_h^t	Vector of bus voltages magnitude of harmonic order h .
V_L^t	Fundamental load buses voltages vector.
x_{cr}^t, x_d^t	Reduction of critical and ordinary load in kW.
x_i	Saved energy of controllable consumer i in kWh.
x_{pv}^t, x_w^t	Reduction of photovoltaic and wind power in kW.
Y_1, Y_h^t	Three-phase bus admittance matrix at fundamental frequency and at harmonic order h .
Z_h^t	Three-phase bus impedance matrix at harmonic order h .
$(Z_{se})_l^h, (Y_{sh})_l^h$	Series Impedance and shunt admittance matrix of three-phase line l at harmonic order h .
ZP_i	Set of zero power exchange time slots for controllable consumer i .

Notation: $(\cdot)^t$ refers to the variable at time slot t , $(\cdot)_{\max}, (\cdot)_{\min}$ for the maximum and minimum allowed limits, $[\cdot]_n$ the element n of the vector, $[\cdot]_{n,m}$ the (n, m) entry of matrix, $[\cdot]_{\{a,b\}}$ the block sub-matrix formed using the sets a, b , $\widehat{a} = \max\{a, 0\}$, $(\cdot)^T$ transposition, $(\cdot)^*$ complex conjugate, $(\cdot)^H$ complex-conjugate-transposition, $\text{Re}\{\cdot\}$ the real part, $\text{Im}\{\cdot\}$ the imaginary part, $\text{Tr}(\cdot)$ matrix trace, $\text{rank}\{\cdot\}$ matrix rank, $|\cdot|$ the magnitude, > 0 positive definite, $j := \sqrt{-1}$, $1_{n \times n}$ identity matrix with dimensions $n \times n$, $0_{n \times m}$ zero matrix with dimensions $n \times m$.

I. INTRODUCTION

QUALITY of power delivered to consumers has gained great attention in recent years. In microgrids, which contain, loads, generation from conventional and renewable sources, and Energy Storage (ES) devices, existence of nonlinear loads may lead to harmonic pollution in bus voltages of other microgrid members. This can cause undesirable effects such as heating, negative sequence torques, and incorrect operation of protection devices. If some microgrid members are sensitive to harmonics in voltage, quality of the delivered power should be concerned in microgrid optimization algorithms.

Energy Management System (EMS) is responsible for centralized optimization of microgrid operation. Intelligent optimization of loads, by optimizing amounts and periods of power exchange and power reduction, is known as Demand Response (DR) [1]–[3].

Microgrids are connected to the main grid through substations and can be operated in either grid-connected mode or islanded mode. Transition between grid-connected and islanded modes may be scheduled, for substation maintenance, for transmission congestion management, or due to insufficient generation at the upstream transmission network. In islanded mode, conventional dispatchable generators are responsible for controlling power balance and frequency, by their own droop

characteristics, and providing reactive power. After removal of the islanding cause, the system returns to grid-connected mode after proper synchronization and this operation may be repeated several times during the scheduling period.

Most of publications in microgrid energy management address optimization in either grid-connected [4], [5] or isolated [6], [7] modes or both modes but as two separate cases as in [1]. In [8], microgrid generators are scheduled for minimizing local generation cost with sufficient reserve to ensure stable islanding without concerning voltage constraints, energy storage, or controllable loads. In [5], [7], and [8], no network model is adopted and the main concern is only balancing between active power generation and consumption.

When dealing with network constraints, such as bus voltages, line currents, line losses, and line power flows, Optimal Power Flow (OPF) is required. Distribution system may also be unbalanced due to phase configurations and unbalanced loading. Unbalance distribution optimal power flow (DOPF) that takes into account constraints on bus voltages is adopted in [9] and [10] for only grid-connected mode and in [11] for islanded mode and both are only for fixed loading snapshot. In [12], network and voltage harmonics constraints are included in the optimization by multiple power flow solutions at fundamental and harmonic frequencies. Two multiple frequency power flow solutions are required to calculate sensitivity of Total Harmonic Distortion of bus voltage magnitudes to injected active or reactive power at each single bus. This constitutes a computational burden. The algorithm in [12] does not provide closed form analytical expressions of power quality and network constraints. Optimization is repeated many times until convergence. Besides, the algorithm is computationally intensive and convergence is not guaranteed.

In this paper, power quality constrained optimization of smart microgrid with nonlinear loads is proposed for scheduled multiple transitions between grid-connected and islanded modes. Loads, generation, and energy storage are scheduled for maximum microgrid profit. Optimization is constrained by acceptable quality of power at microgrid buses in terms of voltage Total Harmonic Distortion (THD). The EMS collects information from smart loads, generators, and grid, performs optimization according to the predetermined schedule of mode transitions, and then sends settings to each microgrid member. Information exchange in the proposed method is shown in figure 1. The main contributions of the proposed method are summarized as follows.

- 1- Microgrid optimization is done for scheduled multiple transitions between grid-connected and islanded modes. Load sharing among generating units, steady-state frequency deviation during islanding, and bidirectional power exchange with grid are considered.
- 2- The algorithm guarantees acceptable quality of power delivered to loads in terms of voltage THD in the presence of nonlinear loads.
- 3- Analytical expressions for power quality constraints as well as network constraints for three-phase unbalanced distribution system are given in closed convex forms

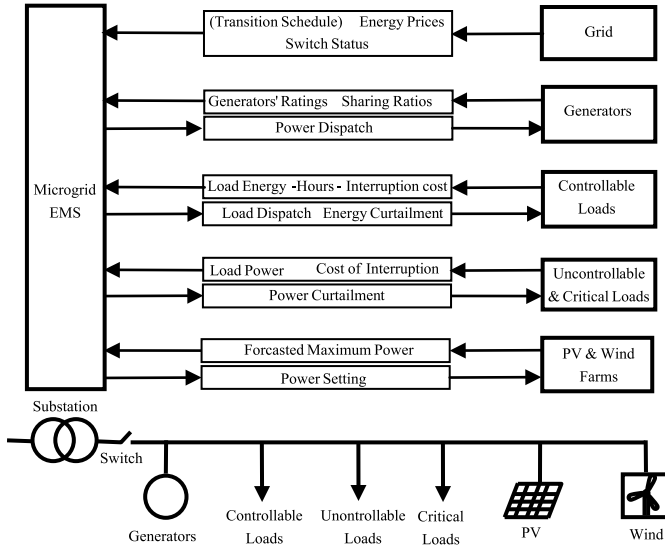


Fig. 1. Information Exchange in the Proposed Smart Microgrid.

without repeated optimizations and multiple power flow solutions as done in [12].

The model proposed in this research can be easily extended to include uncertainty in generation and load using Model Predictive Control (MPC) as in [13], or nonlinear prediction as adopted in [14]. The paper is organized as follows. Problem formulation is presented in Section II. Network and power quality constraints are derived in Section III. Results and discussion are given in Section IV and conclusions are extracted in Section V.

II. PROBLEM FORMULATION

The purpose of the considered optimization is to maximize the microgrid profit and to minimize the cost of power generation, cost of energy purchase from the grid, and cost of load curtailment while satisfying network and power quality constraints.

A. Objective Function

The objective function can be formulated as follows:

$$\begin{aligned} f_{total} = & \sum_{t \in TM} (f_c^t - f_r^t) \hat{p}_{grid}^t + \sum_{t \in TM} (f_g^t p_{grid}^t) \\ & + \sum_{t \in TM} \sum_{g \in G} (f_g^t p_g^t + h_g^t (p_g^t)^2) \\ & + \sum_{i \in C} f_i x_i + \sum_{t \in TM} f_d^t x_d^t + \sum_{t \in TM} f_{cr}^t x_{cr}^t \end{aligned} \quad (1)$$

where $\hat{p}_{grid}^t = \max\{p_{grid}^t, 0\}$. This formulation ensures convexity of the objective function (See [15]). The first two terms represent the cost of energy imported from grid or the profit from energy exported to grid. The third term represents cost of producing energy from local conventional generators. The fourth, fifth and sixth terms represent cost of reduction in controllable, ordinary, and critical loads.

B. Operational Constraints

Energy exchange of controllable loads with grid is only allowed in some hours according to each load type. Power exchange during the other hours should be zero, i.e.,

$$p_i^t = 0 \quad \forall i \in C, \forall t \in ZP_i \quad (2)$$

The sum of power exchanges of each controllable load must equal its energy requirements minus the saved portion.

$$\sum_{t=1}^T p_i^t = E_i - x_i \quad \forall i \in C \quad (3)$$

The storage energy of each controllable load with energy storage is updated by the power exchanges with the microgrid with limits on storage energy and power as follows.

$$SE_i^t = \xi_s SE_i^{t-1} + p_i^t \quad \forall i \in CE \quad \forall t \in TM \quad (4)$$

$$SE_{i \min} \leq SE_i^t \leq SE_{i \max} \quad \forall i \in C \quad \forall t \in TM \quad (5)$$

$$p_{i \min} \leq p_i^t \leq p_{i \max} \quad \forall i \in C \quad \forall t \in TM \quad (6)$$

Minimum limits are negative for controllable loads with energy storage which are allowed to return power to the microgrid and zero otherwise.

Power reduction for ordinary and critical loads is constrained as follows.

$$0 \leq x_d^t \leq P_d^t, 0 \leq x_{cr}^t \leq P_{cr}^t \quad \forall t \in TM \quad (7)$$

For controllable loads, energy reduction is constrained as follows

$$0 \leq x_i \leq E_i \quad \forall i \in C \quad (8)$$

The reduction in generated power for wind and photovoltaic plants must be below the maximum available power obtained using maximum power point tracking (MPPT) control at each time slot.

$$0 \leq x_w^t \leq P_w^t, 0 \leq x_{pv}^t \leq P_s^t \quad \forall t \in TM \quad (9)$$

The maximum apparent power flow through grid transformer must be below its maximum rating.

$$(p_{grid}^t)^2 + (q_{grid}^t)^2 \leq S_{T \max} \quad \forall t \in TM \quad (10)$$

Similarly, for each conventional generator

$$(p_g^t)^2 + (q_g^t)^2 \leq S_{g \max} \quad \forall g \in G \quad \forall t \in TM. \quad (11)$$

C. Constraints for Grid-Connected Periods

During grid-connected mode, power of the conventional generators is shared with predetermined ratios according to their ratings or contracts as follows

$$p_g^t - \lambda_g p_{g+1}^t = 0 \quad \forall g \in G \quad \forall t \in GM \quad (12)$$

Also, there is no reduction in wind or photovoltaic power

$$x_w^t = 0, x_{pv}^t = 0 \quad \forall t \in GM \quad (13)$$

The frequency is fixed and locked to nominal frequency due to the stiff connection with grid, i.e.,

$$\Delta f^t = 0 \quad \forall t \in GM. \quad (14)$$

D. Constraints for Islanded Periods

Islanding causes power imbalance. Conventional generators will be responsible for frequency control through governors with droop constants as follows.

$$p_g^t - p_g^{k_t} - (r_g + d_g)\Delta f^t = 0 \quad \forall g \in G \quad \forall t \in IM \quad (15)$$

Frequency deviation must be constrained between minimum and maximum values as follows

$$\Delta f_{\min} \leq \Delta f^t \leq \Delta f_{\max} \quad \forall t \in IM \quad (16)$$

If a secondary frequency control is used, zero steady-state error is obtained and equations (15) and (16) are replaced by

$$\Delta f^t = 0 \quad \forall t \in IM \quad (17)$$

And balance between generated and consumed power is guaranteed by network constraints (equations (34) to (39)).

Also, during islanded mode, there is no active or reactive power exchange with grid, i.e.,

$$p_{grid}^t = 0, q_{grid}^t = 0 \quad \forall t \in IM. \quad (18)$$

III. NETWORK AND POWER QUALITY CONSTRAINTS

In this section network and power quality constraints are given in closed and convex forms. Convexity ensures global optimality and polynomial convergence time.

A. Network Constraints

Network constraints include nodal active and reactive power equations as well as bus voltage magnitude limits. The nodal injected active and reactive power at any node n satisfy

$$[V_1^t]_n \sum_{m=1}^{n_b} [Y_1^*]_{n,m} [V_1^t]_m^* = P_n^t + jQ_n^t \quad \forall n \in B, \forall t \in T \quad (19)$$

The off-diagonal and diagonal blocks in the three-phase admittance matrix, at fundamental frequency, are formulated as follows; respectively

$$[Y_1]_{\{b1,b2\}} = - \sum_{l \in N_{b1} \cap N_{b2}} \left((Z_{se})_l^1 \right)^{-1} \quad (20)$$

$$[Y_1]_{\{b1,b1\}} = \sum_{l \in N_{b1}} \left((Y_{sh})_l^1 + \left((Z_{se})_l^1 \right)^{-1} \right) \quad (21)$$

The magnitude of node voltages must remain between allowable limits, i.e.,

$$|[V_1]_n|_{\min} \leq |[V_1^t]_n| \leq |[V_1]_n|_{\max} \quad \forall n \in B, \forall t \in TM \quad (22)$$

Constraints (19) and (22) are nonconvex and can be convexified as follows [10].

Assuming that network buses are classified into three-phase grid buses, whose voltages are known, and other n_L non-grid buses with subscript L , the network partitioned nodal equations can be written as follows.

$$\begin{bmatrix} I_{grid}^t \\ I_L^t \end{bmatrix} = \begin{bmatrix} Y_{1(11)} & Y_{1(12)} \\ Y_{1(21)} & Y_{1(22)} \end{bmatrix} \begin{bmatrix} V_{grid}^t \\ V_L^t \end{bmatrix} \quad (23)$$

Solving for voltage of non-grid buses yields

$$V_L^t = Y_{1(22)}^{-1} I_L^t - Y_{1(22)}^{-1} Y_{1(21)} V_{grid}^t \quad (24)$$

Substituting (24) in equation of (23), fundamental frequency bus injected currents can be given by

$$\begin{aligned} I_1^t &= \begin{bmatrix} I_{grid}^t \\ I_L^t \end{bmatrix} = \begin{bmatrix} Y_{1(12)} Y_{1(22)}^{-1} \\ 0_{n_L \times n_L} \end{bmatrix} I_L^t \\ &\quad + \begin{bmatrix} Y_{1(11)} - Y_{1(12)} Y_{1(22)}^{-1} Y_{1(21)} \\ 0_{n_L \times 3} \end{bmatrix} V_{grid}^t \\ &= A_1' I_L^t + A_1'' V_{grid}^t \end{aligned} \quad (25)$$

And fundamental bus voltages are given by

$$\begin{aligned} V_1^t &= \begin{bmatrix} V_{grid}^t \\ V_L^t \end{bmatrix} = \begin{bmatrix} 0_{3 \times n_L} \\ Y_{1(22)}^{-1} \end{bmatrix} I_L^t + \begin{bmatrix} -Y_{1(22)}^{-1} Y_{1(21)} \\ 1_{3 \times 3} \end{bmatrix} V_{grid}^t \\ &= B_1' I_L^t + B_1'' V_{grid}^t \end{aligned} \quad (26)$$

For each node n

$$[I_1^t]_n = a_n^T I_L^t + \alpha_n \quad (27)$$

$$[V_1^t]_n = b_n^T I_L^t + \beta_n \quad (28)$$

where a_n^T , α_n , b_n^T , and β_n are the n^{th} rows of A_1' , $A_1'' V_{grid}^t$, B_1' , and $B_1'' V_{grid}^t$; respectively. Defining

$$K_n^p = \frac{1}{2} (a_n^* b_n^T + b_n^* a_n^T) \quad (29)$$

$$k_n^p = \frac{1}{2} (\beta_n a_n^* + \alpha_n b_n^*) \quad (30)$$

$$\pi_n^p = \text{Re}(\alpha_n^* \beta_n) \quad (31)$$

$$\ddot{K}_n^p = \begin{bmatrix} \text{Re}(K_n^p) & -\text{Im}(K_n^p) \\ \text{Im}(K_n^p) & \text{Re}(K_n^p) \end{bmatrix} \quad (32)$$

$$\dot{k}_n^p = [\text{Re}(k_n^p) \quad \text{Im}(k_n^p)]^T \quad (33)$$

Then the real part of equation (19) can be written in the following convex form [10]

$$\text{Tr}(C_n^p M^t) = P_n^t \quad \forall n \in B, \forall t \in TM \quad (34)$$

$$\text{where } M^t = \begin{bmatrix} I_L^t \\ 1 \end{bmatrix} \left(\begin{bmatrix} I_L^t \\ 1 \end{bmatrix} \right)^H \text{ and } C_n^p = \begin{bmatrix} \ddot{K}_n^p & \dot{k}_n^p \\ (\dot{k}_n^p)^T & \pi_n^p \end{bmatrix}$$

$$M^t \succ 0 \quad (35)$$

$$\text{rank}(M^t) = 1 \quad \forall t \in TM \quad (36)$$

$$[M^t]_{2n_L+1, 2n_L+1} = 1 \quad (37)$$

where I_L^t follows definition (33). A similar procedure can be done for reactive power and voltage magnitude [10] and that yields

$$\text{Tr}(C_n^q M^t) = Q_n^t \quad \forall n \in B, \forall t \in TM \quad (38)$$

$$V_{n \min}^2 \leq \text{Tr}((C_1)_n^v M^t) \leq V_{n \max}^2 \quad \forall n \in B, \forall t \in TM \quad (39)$$

Constraint (36) is nonconvex but it can be omitted because, in most cases, it is satisfied in radial distribution systems [9]. Other constraints, on line power flows, line currents, and line losses can also be included [9]. Equations (34)-(35) and (37) give the required nodal active and reactive power constraints, while equation (39) gives the required bus voltage magnitude constraints all in closed convex format.

B. Harmonics Constraints

Harmonic constraints include limits on Voltage THD at all buses and in all time slots. The injected bus currents at harmonic frequency of order h are related to the fundamental frequency currents, according to the characteristics of each nonlinear load, as follows.

$$\begin{aligned} I_h^t &= K_h I_1^t = K_h (A_1' I_L^t + A_1'' V_{grid}) \\ &= A_h' I_L^t + A_h'' V_{grid} \end{aligned} \quad (40)$$

where $A_h' = K_h A_1'$, $A_h'' = K_h A_1''$ and K_h is a diagonal matrix with $[K_h]_{n,n} = u_h^n e^{j\varphi_h^n}$, representing harmonic to fundamental magnitude ratio and phase angle difference, if a nonlinear load is connected to bus n , and $[K_h]_{n,n} = 0$ otherwise. Harmonic bus voltages are given by

$$\begin{aligned} V_h^t &= Z_h^t I_h^t = Z_h^t (A_h' I_L^t + A_h'' V_{grid}) \\ &= B_h^t I_L^t + B_h'' V_{grid} \end{aligned} \quad (41)$$

where $Z_h^t = (Y_h^t)^{-1}$, $B_h^t = Z_h^t A_h'$, $B_h'' = Z_h^t A_h''$ and Y_h^t is formed the same way as the fundamental frequency admittance matrix taking into consideration the change of imaginary part of series impedance and shunt admittance due to harmonics. For series impedance

$$(Z_{se})_l^h = \text{Re}\{(Z_{se})_l^1\} + jh \text{Im}\{(Z_{se})_l^1\} \quad \forall l \in N \quad (42)$$

Linear loads (critical and ordinary) are converted to constant admittances at harmonic order h . For ordinary load as an example

$$y_h^t = p_d^t - j \frac{1}{h} q_d^t \quad (43)$$

Equation (41) has the same form as (26) and the same procedure leads to

$$\begin{aligned} \text{Tr}((C_h^t)_n^v M^t) &= |[V_h^t]_n|^2 \\ \forall n \in B, \forall t \in TM, \forall h = 3, 5, \dots, h_m \end{aligned} \quad (44)$$

If the maximum allowed THD of bus voltages is THD_{\max} for acceptable power quality at all buses, then

$$\begin{aligned} THD_n^t &= \frac{\sqrt{\sum_{h=3,5,\dots,h_{\max}} |[V_h^t]_n|^2}}{|[V_1^t]_n|} \\ &\leq THD_{\max} \quad \forall n \in B, \forall t \in TM \end{aligned} \quad (45)$$

Squaring the above equation and substituting with (44) gives

$$\begin{aligned} \sum_{h=3,5,\dots,h_{\max}} \text{Tr}((C_h^t)_n^v M^t) &\leq THD_{\max}^2 \text{Tr}((C_1)_n^v M^t) \\ \forall n \in B, \forall t \in TM \end{aligned} \quad (46)$$

Equations (46) are the required power quality constraints.

IV. RESULTS AND DISCUSSION

The proposed optimization method is applied on the unbalanced distribution smart microgrid shown in figure 2. For clarity, each phase is numbered as a separate bus. Rating of substation transformer is 500 kVA and the grid voltage is balanced 380 V, 50 Hz. The microgrid contains three conventional

single phase 50 kVA diesel generators, a 200 kW wind farm, and a 200 kW photovoltaic plant. It is assumed that conventional generators have both primary and secondary frequency control and that there is no damping or frequency-dependent loads. The wind farm and photovoltaic plants are assumed to be controlled by MPPT. The maximum available power profile for the wind farm and photovoltaic plant are obtained from [3] and [16]; respectively. Wind and photovoltaic plants operate at unity power factor and reactive power is only supplied from conventional generators and grid. The loads in the microgrid are three types. The first type contains three single phase controllable loads with nominal energy consumption of 250, 500, and 750 kWh with unity power factor. The maximum power exchanged by each load is limited to 50 kW at each hour. The available hours of loads are 3→19, 4→20, and 5→21; respectively. Only the first controllable load has energy storage and is allowed to regenerate power to grid. Energy storage is limited to between 5% and 200% of its nominal energy consumption and the initial storage is assumed to be 100% of its nominal energy consumption. The second type of loads is an ordinary uncontrollable load with the daily active power profile shown in figure 3(b) [17]. This load is three-phase unbalanced and is distributed among the three phases with ratio 40%, 30%, and 30%. The third type is a single phase critical uncontrollable load with a fixed power of 12.5 kW for the first 16 hours and 25 kW for the last 8 hours and is connected to phase c of the ordinary load three-phase bus. Power factor of both ordinary and critical load is 0.8 lagging. The cost of purchasing energy from grid is assumed to follow the daily profile shown in figure 3(a) [2]. The time slot is taken as one hour and so, energy cost is treated as power cost. The price of selling power to grid is assumed to be 90% of the energy cost at each hour. The cost of dropping a single kWh of each controllable load, reducing a single kW of ordinary and critical load are taken as 85%, 95%, and 98%; respectively of maximum cost of purchasing energy from grid during the day. This gives $f_i = 0.0382$, $f_d^t = 0.0427$, and $f_{cr}^t = 0.0441$. The linear cost coefficients of the three generators are taken as 70%, 60%, and 50%; respectively of the minimum price of selling energy to grid and the quadratic terms are taken as half the linear terms. This gives $f_{g1} = 0.0158$, $h_{g1} = 0.0079$, $f_{g2} = 0.0135$, $h_{g2} = 0.0067$, $f_{g3} = 0.0113$, and $h_{g3} = 0.0056$. Segments between buses are assumed equal in length and all have three-phase series impedance of

$$Z_s = \begin{bmatrix} 0.0693 + j0.2036 & 0.0312 + j0.1003 & 0.0316 + j0.0847 \\ 0.0312 + j0.1003 & 0.0675 + j0.2096 & 0.0307 + j0.0770 \\ 0.0316 + j0.0847 & 0.0307 + j0.0770 & 0.0683 + j0.2070 \end{bmatrix}$$

per-unit based on 500 MVA base and shunt admittances are neglected [9]. The scheduling period is one day. The microgrid is assumed to start in grid-connected mode and then three mode transitions occur at the beginning of the 8th, 11th, 13th, and 14th hours. Controllable loads are assumed harmonic producing sources with the characteristics shown in table I [18]. Without loss of generality of the algorithm, renewable sources are assumed non producing sources by using advanced inverter modulation techniques and/or harmonic filters. During islanded mode, conventional generators

TABLE I
CHARACTERISTICS OF HARMONIC SOURCES [18]

h	3	5	7	9	11	13	15
u_h^n	0.542	0.152	0.069	0.043	0.036	0.029	0.025
ϕ_h°	2.2	112.3	153.4	-93.5	-12.4	96.7	-181.2

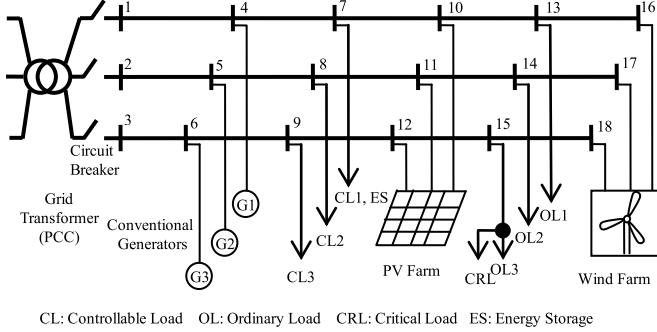


Fig. 2. Microgrid Test System.

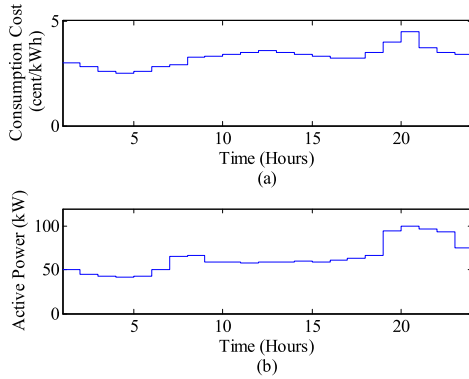


Fig. 3. Energy Cost and Uncontrolled Load Power; (a): Energy cost, and (b): Load Power.

maintain voltages of PCC at their nominal values. The optimization is performed using the convex programming tool CVX [15] which is a MATLAB-based optimization tool with SDP3 solver. According to IEEE standard [19], THD must be below 5%. For harmonic sensitive loads, the limit can be made lower. In simulation, six test cases are considered; the unconstrained THD case and five cases corresponding to THD_{max} form 1% to 5%.

Figures 4–9 give the results of the case of 3% THD limit. Active and reactive power exchange with grid is shown in figures 4(a), and 4(b). Power is exported to grid at periods of higher energy rate, higher renewable generation, and lower load. Frequency is shown in figure 4(c) and it is fixed at 50 Hz during grid-connected mode and also during islanding mode due to secondary frequency control. Power exchange, and storage energy of the controllable load with energy storage are shown in figure 5(a), and 5(b); respectively and they show that both power and stored energy remain within their allowable limits. Discharging periods of energy storage coincides with periods of power export to grid. The daily consumed power of the other two controllable loads are shown

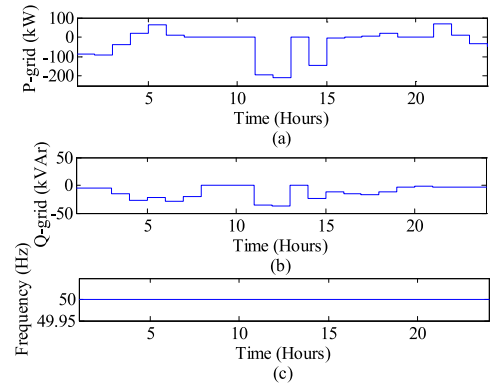


Fig. 4. Grid Active Power, Reactive Power and Frequency; (a): Grid Active Power, (b) Grid Reactive Power, and (c): Frequency.

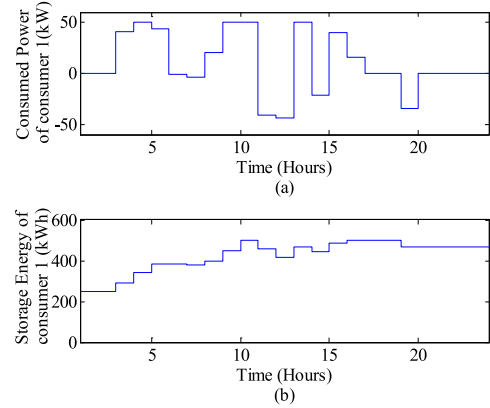


Fig. 5. Consumed Power and Energy Storage of controllable load 1; (a): Consumed Power, and (b): Energy storage.

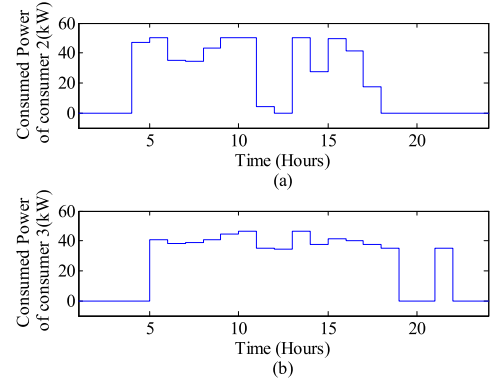


Fig. 6. Power of controllable loads 2, and 3; (a) Load 2, and (b): Load 3.

in figure 6(a), and 6(b); respectively. Controllable loads consumption is shifted to periods with lower ordinary and critical loads and lower energy rates. The first and third controllable loads are curtailed as shown in table II. The ordinary load power is reduced by 46.15 kW at hour 20 and there is no reduction in critical load during scheduling period. The actual and maximum available wind power are shown in figure 7(a) and those of photovoltaic generation are shown in figure 7(b). Wind power is reduced at both islanded periods.

In grid connected periods, both wind and photovoltaic farms are operated at maximum available power for maximum microgrid profit by injecting power to the grid.

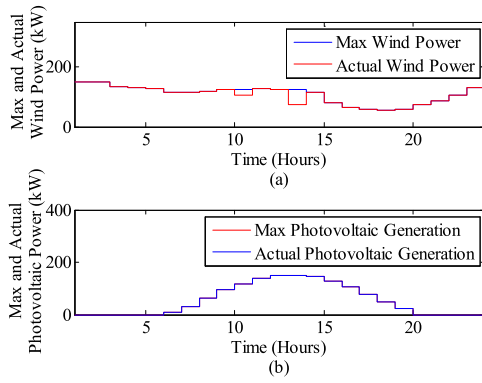


Fig. 7. Maximum and Actual Renewable Generation; (a): Wind, and (b): Photovoltaic.

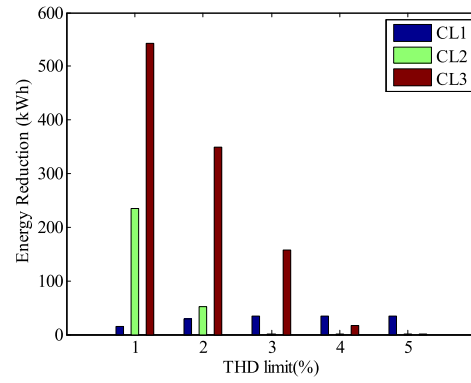


Fig. 10. Reduction in controllable Loads at different THD limits.

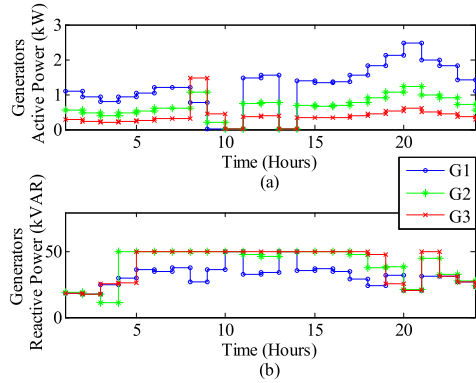


Fig. 8. Generators Active and Reactive Power; (a): Active Power, and (b): Reactive Power.

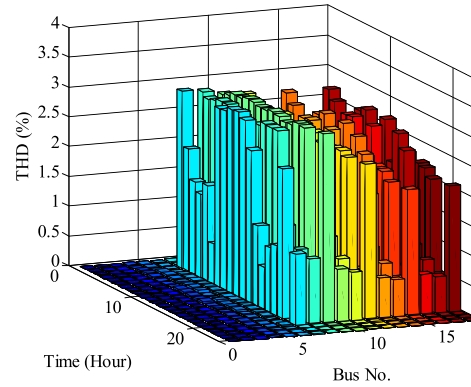


Fig. 11. THD of Buses during the Day at 3% Limiting THD.

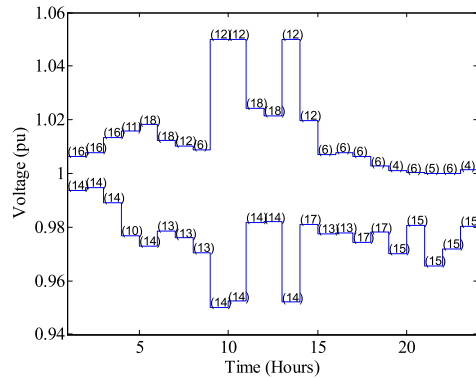


Fig. 9. Maximum and Minimum Bus Voltages and Corresponding Buses.

Active and reactive power injected by conventional generators are shown in figure 8(a), and 8(b); respectively. Active power is shared by the assigned ratios during grid-connected periods.

Maximum and Minimum Voltage magnitude at all buses in the scheduling period are shown in figure 9 with the corresponding bus numbers. It is clear that all voltages stay within the allowed limits. It is also noted that bus 12 has the maximum voltage during the scheduling period because of maximum power generation of the photovoltaic station while bus 14 has the lowest voltage because of the maximum power consumption of uncontrolled load.

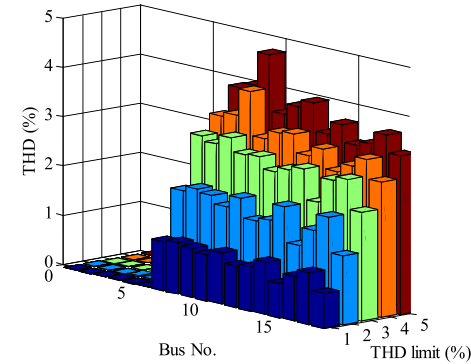


Fig. 12. THD of Buses at Hour 10 for Different THD Limits.

Figure 10 shows curtailment in controllable loads at different limiting THD. The curtailment increases for reduced limiting THD to comply with the more restricting constraint. Total harmonic distortion at all network buses during the day for 3% limiting THD is shown in figure 11. THD of all buses is within the limits and they increase at periods of controllable loads power exchange. THD of all buses at different limiting THDs at hour 10 is shown in figure 12. THD is higher at controllable loads buses and they get lower at far buses. Effect of limiting THD on microgrid economics is demonstrated in table II. It is found that wind utilization factor is lower than that of solar because of the reduction in wind power at islanding periods to limit the voltage magnitude at upstream buses.

TABLE II
COMPARISON BETWEEN DIFFERENT LIMITING THDS

Limiting THD	1%	2%	3%	4%	5%	Unconstrained
Total Consumption	2.6255 MWh	3.0535 MWh	3.3364 MWh	3.493 MWh	3.516 MWh	3.5189 MWh
Total Consumption Cost	86.2637 \$	99.9602 \$	108.8024 \$	113.647 \$	114.3473 \$	114.423 \$
Net Grid bill	27.078 \$	23.1994 \$	19.2067 \$	15.3623 \$	14.8568 \$	14.8584 \$
Net Microgrid Profit	-6.3549 \$	3.5281\$	8.6215 \$	10.1578\$	10.2651 \$	10.2682 \$
Wind Utilization Factor	90.1078 %	95.059 %	97.4942 %	98.3641 %	98.3565 %	98.3095 %
Solar Utilization Factor	97.2504 %	100 %	100 %	98.6123 %	98.6277 %	98.7294 %
Saved Energy from Controllable Loads	(14.58, 235.25, 543.42) kWh	(29.33, 51.98, 349.58) kWh	(34.41, 0, 158.32) kWh	(34.41, 0, 15.89) kWh	(34.41, 0, 0) kWh	(34.41,0,0) kWh
Saved Power form Fixed Load	46.1476 kW at hour 20	46.1476 kW at hour 20	46.1476 kW at hour 20	46.1476 kW at hour 20	46.1476 kW at hour 20	46.1476 kW at hour 20
Cost of Energy Interruption to Controllable Loads	30.3414 \$	16.4815 \$	7.3716 \$	1.9241 \$	1.316 \$	1.3161 \$
Cost of Power Interruption to Ordinary Loads	1.9728 \$	1.9728 \$	1.9728 \$	1.9728 \$	1.9728 \$	1.9728 \$

A more restricting THD leads to less microgrid profit, less total consumption, less renewable utilization, and more reduction in controllable loads. On the other hand, results of the 5% limiting THD provides no remarkable change with respect to the unrestricted case. The maximum THD for the unrestricted case is 6.29% (not shown in table) which is slightly above the 5% limit. Compromise should be made by the EMS between microgrid economics and sensitivity of microgrid members to voltage harmonics.

REFERENCES

- [1] W. Shi, X. Xie, C.-C. Chu, and R. Gadh, "Distributed optimal energy management in microgrids," *IEEE Trans. Smart Grid*, vol. 6, no. 3, pp. 1137–1146, May 2015.
- [2] K. M. Tsui and S. C. Chan, "Demand response optimization for smart home scheduling under real-time pricing," *IEEE Trans. Smart Grid*, vol. 3, no. 4, pp. 1812–1821, Dec. 2012.
- [3] K. Christakou, D.-C. Tomozei, J.-Y. Le Boudec, and M. Paolone, "GECN: Primary voltage control for active distribution networks via real-time demand-response," *IEEE Trans. Smart Grid*, vol. 5, no. 2, pp. 622–631, Mar. 2014.
- [4] D. T. Nguyen and L. B. Le, "Joint optimization of electric vehicle and home energy scheduling considering user comfort preference," *IEEE Trans. Smart Grid*, vol. 5, no. 1, pp. 188–199, Jan. 2014.
- [5] Y. Levron, J. M. Guerrero, and Y. Beck, "Optimal power flow in microgrids with energy storage," *IEEE Trans. Power Syst.*, vol. 28, no. 3, pp. 3226–3234, Aug. 2013.
- [6] J. Pahasa and I. Ngamroo, "PHEVs bidirectional charging/discharging and SoC control for microgrid frequency stabilization using multiple MPC," *IEEE Trans. Smart Grid*, vol. 6, no. 2, pp. 526–533, Mar. 2015.
- [7] T. T. Gamage *et al.*, "A novel flow invariants-based approach to microgrid management," *IEEE Trans. Smart Grid*, vol. 6, no. 2, pp. 516–525, Mar. 2015.

- [8] S.-J. Ahn, S.-R. Nam, J.-H. Choi, and S.-I. Moon, "Power scheduling of distributed generators for economic and stable operation of a microgrid," *IEEE Trans. Smart Grid*, vol. 4, no. 1, pp. 398–405, Mar. 2013.
- [9] E. Dall'Anese, H. Zhu, and G. B. Giannakis, "Distributed optimal power flow for smart microgrids," *IEEE Trans. Smart Grid*, vol. 4, no. 3, pp. 1464–1475, Sep. 2013.
- [10] T. Erseghe and S. Tomasin, "Power flow optimization for smart microgrids by SDP relaxation on linear networks," *IEEE Trans. Smart Grid*, vol. 4, no. 2, pp. 751–762, Jun. 2013.
- [11] D. E. Olivares, C. A. Canizares, and M. Kazerani, "A centralized energy management system for isolated microgrids," *IEEE Trans. Smart Grid*, vol. 5, no. 4, pp. 1864–1875, Jul. 2014.
- [12] M. Hong, X. Yu, N.-P. Yu, and K. A. Loparo, "An energy scheduling algorithm supporting power quality management in commercial building microgrids," *IEEE Trans. Smart Grid*, vol. 7, no. 2, pp. 1044–1056, Mar. 2016.
- [13] T. Wang, D. O'Neill, and H. Kamath, "Dynamic control and optimization of distributed energy resources in a microgrid," *IEEE Trans. Smart Grid*, vol. 6, no. 6, pp. 2884–2894, Nov. 2015.
- [14] M. Marzband, F. Azarnejadian, M. Savaghebi, and J. M. Guerrero, "An optimal energy management system for islanded microgrids based on multiperiod artificial bee colony combined with Markov chain," *IEEE Syst. J.*, to be published.
- [15] CVX: *MATLAB Software for Disciplined Convex Programming*. Accessed on Apr. 4, 2015. [Online]. Available: <http://cvxr.com/cvx/>
- [16] O. Homaei, A. Zakariazadeh, and S. Jadid, "Real-time voltage control algorithm with switched capacitors in smart distribution system in presence of renewable generations," *Int. J. Elect. Power Energy Syst.*, vol. 54, pp. 187–197, Jan. 2014.
- [17] X. Liu, A. Aichhorn, L. Liu, and H. Li, "Coordinated control of distributed energy storage system with tap changer transformers for voltage rise mitigation under high photovoltaic penetration," *IEEE Trans. Smart Grid*, vol. 3, no. 2, pp. 897–906, Jun. 2012.
- [18] R. Abu-Hashim *et al.*, "Test systems for harmonics modeling and simulation," *IEEE Trans. Power Del.*, vol. 14, no. 2, pp. 579–587, Apr. 1999.
- [19] *IEEE Recommended Practices and Requirements for Harmonic Control in Electrical Power System*, IEEE Standard 519, 1992.

Karim Hassan Youssef was born in Alexandria, Egypt, in 1981. He received the B.Sc., M.Sc., and Ph.D. degrees in electrical engineering from Alexandria University, Alexandria, in 2003, 2005, and 2009, respectively. He is an Assistant Professor with the Electrical Engineering Department, Faculty of Engineering, Alexandria University. His current research interests include distribution system design, control and automation, power system control, and renewable energy. He was a recipient of the Egyptian Government Award for his Ph.D. dissertation.